Fatigue & Fracture of Engineering Materials & Structures 1998; **21**: 411–423

PREDICTING THE EFFECTS OF LOAD RATIO ON THE FATIGUE CRACK GROWTH RATE AND FATIGUE THRESHOLD

G. A. KARDOMATEAS and R. L. CARLSON

School of Aerospace Engineering, Georgia Institute of Technology, Altanta, Georgia 30332-0150, USA

Abstract—The effect of the load ratio, R, on fatigue crack growth behaviour is analysed on the basis of the recently proposed inelastic discrete asperities model. A wide range of load ratios, both positive and negative, are examined. Particular emphasis is placed on compressive excursions, i.e. negative R loadings. The inelastic discrete asperities model is a micro-mechanical analysis based on the plastic crushing of a single asperity (or multiple asperities) located on the crack face close to the crack tip and under dominantly plane strain conditions. Experimental data have indicated that the primary crack face contacts which obstruct closure are immediately adjacent to the crack tip, although segments of the crack face more distant from the crack tip are not neglected. However, the more distant asperities are a part of the past crack advance history which does not influence current behaviour. By use of this model, it is shown that the effect of the load ratio can be adequately predicted once some baseline information on mechanical material properties and surface roughness is provided. The model also provides useful trend information and explains many of the observed phenomena, e.g. the 'saturation' of the compressive underload effects. For a constant applied nominal stress intensity factor range, ΔK_{nom}, it is shown that the effective stress intensity factor range, ΔK_{eff}, initially decreases as the positive R decreases (corresponding to the increasing influence of closure), reaches a minimum around $R = 0$, and then starts increasing with negative R (corresponding to the plastic crushing of the asperities which reduces closure), eventually reaching a saturation level below ΔK_{nom}. Conversely, for an assumption of a constant ΔK_{eff}, the applied ΔK_{nom} increases as the positive load ratio decreases, reaching a maximum around $R = 0$, and then decreases with more negative R values, eventually reaching again a saturation level (above ΔK_{eff}). It is also shown that the effect of material hardness can be directly analysed based on this model.

Keywords—Fatigue crack growth; Load ratio; Fatigue threshold; Inelastic discrete asperities; Compressive excursions; Stress intensity factor range.

INTRODUCTION

It is well established that the load ratio, R, defined as the ratio of the algebraically minimum over the maximum load, affects the fatigue crack growth and threshold behaviour, e.g. [1]. If the load ratio is positive, experiments have shown that the required stress intensity factor range for growth decreases with increasing positive R values. Several authors have proposed empirical equations to describe the dependence of the threshold value on R, e.g. McEvily [2]. It is generally recognized that a phenomenon of major influence in this issue is the decrease in the contribution of crack closure as the positive load ratio increases.

On the other hand, if the load ratio is negative, it has been observed that the required stress intensity factor range for growth (threshold stress intensity range) decreases as R becomes more negative, and after a certain point, it remains constant ('saturation' level), e.g. [3]. In fact, the common analytical practice has been to exclude the compression segments since it seems reasonable to believe that no contribution to crack growth is developed during a compressive excursion. Thus, for a negative load ratio, R cycle, the stress intensity factor range is set equal to the maximum stress intensity factor. This is based on the assumption that a crack would be closed in compression and only the tensile portion of the loading cycle can contribute to crack growth. However, a common conclusion from a number of experimental programs during the past several years, has been that the use of the foregoing assumption of neglecting the compressive segment may lead to non-conservative predictions. A review of the results from these experimental investigations on

both smooth bars and cracked specimens can be found in Carlson and Kardomateas [4]. For example, Zaiken and Ritchie [5] observed crack growth below the threshold stress intensity range after the application of large compression overloads.

Since much of the observed near-threshold behaviour can be attributed to the closure phenomenon, many studies have been performed in an attempt to understand the effect of surface roughness on fatigue crack growth. The closure obstruction effect of a plastic wake generated as a crack advances was analysed by Budiansky and Hutchinson [6]. They used a Dugdale strip model as a basis for their analysis, and demonstrated that a wake in the form of a plastic layer could obstruct closure and therefore reduce the effective range of the stress intensity factor. Budiansky and Hutchinson [6] considered the case of plane stress. Subsequently, Newman [7] extended the use of a Dugdale strip model by introducing a crack advance criterion and treating the plane strain case.

Dugdale strip models result in the production of plastic layers which are in continuous contact along the crack faces. Tack and Beevers [8], however, have presented micrographic evidence that gaps remain between crack faces even under compressive loading. Also, Buck *et al.* [9] used acoustic wave techniques to show that crack face contact occurs at discrete points. These observations suggest that a discrete asperity model for closure can be useful in diagnosing the mechanics of closure obstruction.

With regard to compressive load excursions, it is reasonable to expect that the height of individual asperities can be reduced by crushing, whereas the compressive loading would be less effective in reducing the height of a continuous layer for the plane strain case. The crushing of closure obstacles would qualitatively explain the observations of increased crack growth rate following compressive excursions [1].

In a fundamental paper, Forsyth [10] suggested that the topography of a fracture surface near the crack tip, as well as the externally applied loads, was important to an understanding of crack advance. Modelling surface features, e.g. asperities which act as obstructions to closure leads to a partitioning of the crack tip stress state into two components, i.e. a component caused by external forces which may be classified as global, and one resulting from asperity contact forces which may be termed local. Since there are a variety of local contact force types that can be developed, different crack tip states are possible.

Based on these observations, a single asperity model based on the elastic compression of an asperity was formulated by Beevers *et al.* [11]. The single asperity model is an idealization in which complete closure is prevented at one point near the crack tip. As the external load decreases, and the upper and lower fracture surfaces approach one another, however, it seems likely that additional asperity contacts, more distant from the crack tip, would also develop. A multiple asperity model, again based on the elastic compression of the asperities, was presented by Carlson and Beevers [12].

These discrete asperities models provide a rational explanation of the observed behaviour due to closure obstruction in load sequences that involve cycling in tension with a positive load ratio, and involve mostly elastic loading/unloading of the asperities. In order to adequately explain the phenomena associated with compressive excursions of sizeable magnitude, a model accounting for the plastic crushing of the asperities was presented recently by Kardomateas and Carlson [13,14] for both a single or multiple asperity contact.

In this work, both positive and negative load ratios are examined through the inelastic discrete asperities model with emphasis placed on explaining the near-threshold fatigue behaviour. It is clearly proven why for positive Rs, the required applied stress intensity range, ΔK_{nom}, for growth, increases as the positive load ratio decreases, and why for negative load ratios, the required ΔK_{nom}

for growth decreases with more negative Rs. It is also demonstrated that positive values of stress intensity can be developed with externally applied compressive forces, and it is clearly explained why the 'saturation' phenomenon associated with the effect of negative load ratios occurs.

THE INELASTIC DISCRETE ASPERITIES MODEL

For the plane strain case, the distribution of the asperities is essentially uniform across the specimen thickness, which suggests the possibility of representing the asperities configuration through the thickness by an effective (through-thickness) line contact. The line contact representation permits the problem to be treated as a two-dimensional one.

The essential features of the model are shown in Fig. 1. Consider an asperity at a distance C from the crack tip in a specimen of thickness t. The presence of both externally applied forces and crack face forces is illustrated in Fig. 1(a), whereas the details of the proposed model are indicated in Fig. 1(b). Only the upper crack face is shown. A force P develops on the asperity when it is in contact. The initial asperity height is L_0 and the final, compressed height is L_f. Similarly, the initial asperity width is b_0 and the final, compressed one is b_0. Asperity size and spacing is typically a fraction of the grain size. Finally, let us denote by t the asperity thickness.

The total mode I stress intensity factor at the crack tip depends on the local crack force P, and the external or global loading. The stress intensity factor produced by a concentrated, opposing line load on the crack faces of a finite centre crack of length $2a$, can be determined from Sih *et al.* [15]. The opening mode stress intensity factor for plane strain in terms of the local crack face force is:

$$K_{\mathrm{I,local}} = \left(\frac{1}{\pi C}\right)^{1/2}\left(2 - \frac{C}{a}\right)^{1/2}\frac{P}{t} \tag{1}$$

This expression is also valid for a single-edge crack of length a (this can be easily shown by following the same procedure as in Sih *et al.* [15].

The contribution of the external load will be represented by $K_{\mathrm{I,global}}$. By superposition, the total

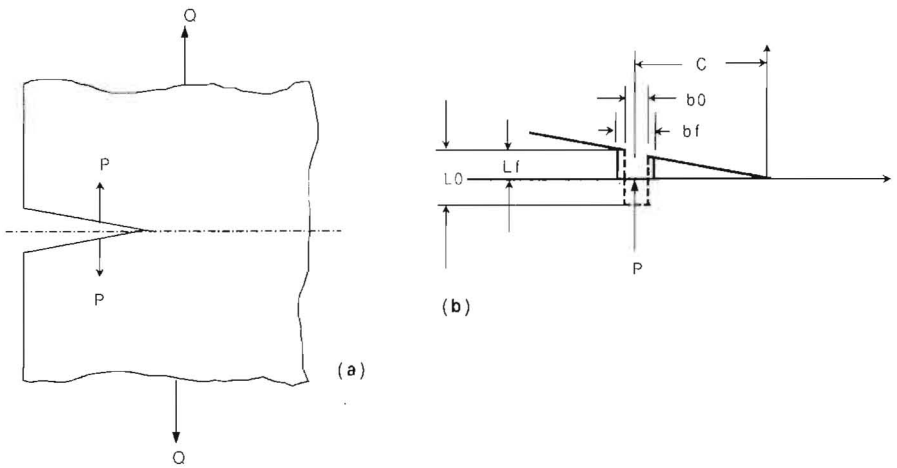

Fig. 1. Cracked body configuration: (a) external (global) and crack tip (local) loading; (b) a single asperity on the upper crack face.

stress intensity factor is

$$K_I = K_{I,\text{local}} + K_{I,\text{global}} \tag{2}$$

The dimension L_0 represents the initial magnitude of the interference produced by the asperity. The effective initial width of the asperity is b_0 [Fig. 1(b)]. Since the asperity may be re-loaded at subsequent cycles after being partially crushed, the i subscript will be used to denote the current (after the i-th cycle) dimensions, e.g. L_i instead of L_0.

The load P will now be determined form a displacement condition at the asperity site, which includes the plastic crushing of the asperity.

The vertical displacement at the upper crack face, i.e. at $\theta = \pi$ and an arbitrary r, is:

$$U_2(r, \pi) = U_{2,\text{global}} + U_{2,\text{local}} \tag{3}$$

By use of the stress intensity factors for the global and local load, we can write the displacement at the asperity site, $r = C$, $\theta = \pi$:

$$U_2(C, \pi) = \frac{2}{G}\left(\frac{C}{2\pi}\right)^{1/2}(1-\nu)K_{I,\text{global}} + \frac{2(1-\nu)}{\pi G}\left(1 - \frac{C}{2a}\right)^{1/2}\frac{P}{t} \tag{4}$$

where G is the shear modulus and ν is the Poisson's ratio.

Hence, the first condition for determining the forces P is the displacement at the asperity site

$$U_2(C, \pi) = L_f \tag{5}$$

Since L_f is not known, let us consider now the relations between the interference height during closure L_f and asperity force P.

The asperity is assumed under uniaxial compression σ (all other stress components are zero). Moreover, the total equivalent strain of the asperity is

$$\bar{\varepsilon}^T = \bar{\varepsilon}^e + \bar{\varepsilon}^p \tag{6}$$

where $\bar{\varepsilon}^e$ is the elastic and $\bar{\varepsilon}^p$ the plastic component (we consider the asperity stress σ and strain ε to be positive when they are compressive). Notice that in uniaxial compression, although there are other non-zero components of strain, i.e. $\varepsilon_{11} = \varepsilon_{33} = -\varepsilon_{22}/2$, it turns out that $\bar{\varepsilon} = \varepsilon_{22}$. Hence, since

$$\bar{\varepsilon}^e = \sigma/E; \qquad \bar{\varepsilon}^T = \ln\frac{L_0}{L_f} \tag{7}$$

the plastic strain component is

$$\bar{\varepsilon}^p = \ln\frac{L_0}{L_f} - \frac{\sigma}{E} \tag{8}$$

where E is the modulus of elasticity. Assume now an equivalent true stress versus integrated equivalent plastic strain law

$$\bar{\sigma} = \sigma_0(\varepsilon_0 + \bar{\varepsilon}^p)^n \tag{9}$$

where n is the strain hardening exponent. Let us denote by $A_0 = tb_0$ the initial cross-sectional area of the asperity. For simplicity, we shall again consider the material as being incompressible in both the elastic and plastic ranges when cross-sectional area calculations are performed (this would be strictly accurate if the Poisson's ratio is 0.5; however the effort introduced for the usual value of 0.3 can be reasonably expected to be small, if the elastic strains are small compared to the plastic

ones). Therefore, using the incompressibility requirement $A_f L_f = A_0 L_0$, to obtain a relationship for the current cross-section A_f, and the stress $\sigma = P/A_f$, and subsequently, substituting in Eqs (7) and (8), gives one equation in P, L_f:

$$\left[\frac{PL_f}{\sigma_0 A_0 L_0}\right]^{1/n} = \ln\frac{L_0}{L_f} - \frac{PL_f}{EA_0 L_0} + \varepsilon_0 \tag{10a}$$

If the asperity is compressed below yield, then the foregoing equation is replaced with

$$\frac{P}{EA_i} = 1 - \frac{L_f}{L_i} \tag{10b}$$

where L_i, A_i are the current (after the i-th cycle) asperity height and cross-sectional area when the asperity is re-loaded.

The other equation needed to solve for L_f and P is found by combining Eqs (4) and (5):

$$L_f = \frac{2}{G}\left(\frac{C}{2\pi}\right)^{1/2}(1-\nu)K_{1,\text{global}} + \frac{2(1-\nu)}{\pi G}\left(1-\frac{C}{2a}\right)^{1/2}\frac{P}{t} \tag{11}$$

Notice that the final, crushed asperity width can be found from the volume preservation condition and transverse strain equality $\varepsilon_{11} = \varepsilon_{33}$ (if 2 denotes the axial direction):

$$b_f = b_0\sqrt{L_0/L_f} \tag{12}$$

If the asperity is loaded elastically, then eliminating L_f leads to the following linear equation for determining P:

$$P\left[\frac{L_i}{EA_i} + \frac{2(1-\nu)}{G\pi t}\left(1-\frac{C}{2a}\right)^{1/2}\right] = L_k - \frac{2(1-\nu)}{G}\left(\frac{C}{2\pi}\right)^{1/2}K_{1,\text{global}} \tag{13}$$

The description of the asperity behaviour for the two separate phases, i.e. the loading and unloading one, will follow next, by reference to Fig. 2.

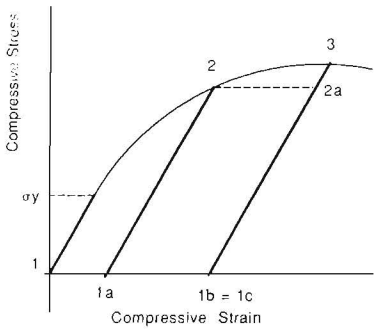

Fig. 2. Schematic of asperity loading/unloading behaviour.

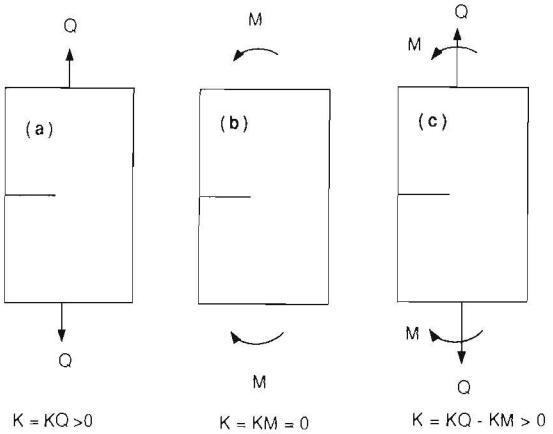

Fig. 3. Illustrating the negative contribution of a closing bending moment on the stress intensity factor: (a) pure tension, (b) pure bending, and (c) combined tension and bending.

Loading phase

During the application of the external cyclic load, Q, asperity loading may occur from the initial configuration or it may involve re-loading after the asperity has been plastically crushed to a reduced height. Hence, during the decreasing external load cycle (loading the asperity) from a general position $(Q_i, P_i = 0, L_i, A_i)$ to a position $(Q_f < Q_i, P, L_f \leqslant L_i, A_f \geqslant A_i)$, the following conditions may develop:

(i) No asperity contact takes place and $K_I = K_{I,global}$ if, from Eq. (11):

$$\frac{2(1-\nu)}{G}\left(\frac{C}{2\pi}\right)^{1/2} K_{I,global} > L_i \tag{14}$$

(ii) If the foregoing condition is not met, and contact of the asperity takes place, the following numerical solution procedure is followed: for a specific L_f, determine P so that the constitutive of the asperity [either elastic or plastic, Eq. (10)] is satisfied. Finally, iterate through values of L_f so that P, so-determined, satisfies the displacement condition, Eq. (11).

In each of the previous steps, to determine the force P that corresponds to a final asperity height L_f, first examine if elastic compression take place. This would occur if:

$$P = EA_i\left(1 - \frac{L_f}{L_i}\right) < P_u \tag{15}$$

where P_u is the load from which the asperity was unloaded, or the yield load if no previous plastic loading was involved. If the condition of Eq. (15) is not satisfied, then the plastic constitutive equation [Eq. (10a)] is numerically solved; the search starts from the elastic limit, i.e. with $L_{min} = L_i - P_u L_i/(EA_i)$.

In all cases, the local stress intensity factor is given in terms of the asperity load, P, by Eq. (1) and the total (global and local) stress intensity factor by Eq. (2). Notice again that the current asperity height, L_i, and cross-sectional area, A_i, are sometimes needed instead of the initial values, L_0 and A_0, respectively since on re-loading after a compressive excursion, the asperity is loaded elastically from the current (crushed asperity) dimensions.

Unloading phase

During the increasing external load cycle (unloading the asperity to zero asperity load, e.g. 2-1a or 3-1c in Fig. 2), from a position (Q_f, P_u, L_f, A_f) to a position $(Q_i > Q_f, P = 0, L_i > L_f, A_i < A_f)$, we recover not the initial asperity height L_0, but the final compressed one, L_f, plus the change in height that is given by the elastic solution that corresponds to the load P_u at which unloading of the asperity takes place, i.e.:

$$L_i = L_f + \frac{P_u L_f}{EA_f}; \qquad A_i = L_0 A_0 / L_i \tag{16}$$

Notice that L_i is now the 'new' (after unloading) interference height.

Moreover, we do not recover the initial cross-sectional area and asperity width, but the final crushed asperity one, minus the elastic recovery, which can again be found by use of Eq. (16).

An important but saddle point of this analysis will now be discussed. Since the crack will always be open due to the asperity interference, during the compressive segment of the applied load cycle, i.e. when $Q < 0$, there is a negative contribution of the external load to the stress intensity factor, i.e. $K_{I,global}$ has a negative sign and is calculated by the same relation as for a positive external load. An analogous way to envision this is to consider the same single-edge cracked configuration

when an opening tensile loading Q is first applied, and then a closing bending moment M is applied (Fig. 3). A pure bending moment M, applied alone, would result in zero stress intensity, $K = K_M = 0$. On the contrary, a pure tensile load, applied alone, would give a non-zero $K = K_Q > 0$. The combined case, however, would have a stress intensity $K = K_Q - K_M > 0$, i.e. it would entail a 'negative' contribution of the closing bending moment M. Hence, a 'negative K' can contribute, if the crack is open.

OPENING AND ZERO LOAD STRESS INTENSITIES

An important benchmark quantity in closure analyses is the opening stress intensity factor, K_{open}, at which asperity contact is first established when the load is decreasing. This can be found by setting $P = 0$ in Eq. (11):

$$K_{open} = \frac{L_i G}{2(1-\nu)} \left(\frac{C}{2\pi} \right)^{-1/2} \tag{17}$$

where L_i is the current asperity height. Also, the opening load (external load at which asperity contact is established), Q_{open}, can be found from solving $K_{open} = K_I(Q_{open})$.

It has been suggested that the effective range be calculated as:

$$\Delta K_{eff} = K_{max} - K_{min} \quad \text{for the case of} \quad K_{open} < K_{min} \quad \text{for} \quad R > 0$$

and

$$\Delta K_{eff} = K_{max} - K_{open} \quad \text{for the case of} \quad K_{open} > K_{min} \quad \text{for} \quad R > 0$$

The last relation has also been suggested to be used for negative R values, but the present model indicates that this may not provide adequate accuracy since K_{open} in Eq. (17) is based on the asperity height before the excursion, and this height is further reduced by plastic crushing during the compressive excursion with an associated change of the prevailing effective stress intensity factor at minimum load.

Another benchmark quantity is the zero load stress intensity factor, K_0, which corresponds to zero applied external load, $Q = 0$. For completely elastic behaviour, at $K_{I,global} = 0$, Eqs (13) and (1) give:

$$K_{0,el} = K_{I,local} = \left(\frac{2}{\pi C} \right)^{1/2} \left[\frac{1}{Eb} + \frac{2(1-\nu)}{\pi G L_0} \left(1 - \frac{C}{2a} \right)^{1/2} \right]^{-1} \tag{18}$$

If the plastic crushing of the asperity is included, then the zero load stress intensity factor, $K_{0,pl}$, should be determined by following the procedure for calculation of the asperity load P and the final asperity height L_f, as this has been previously outlined, i.e. by solving Eqs (10) and (11). In general, Eq. (18) results in a $K_{0,el}$ close to the opening value, K_{open}; however, inclusion of the plasticity effects would predict that the zero load value of the stress intensity, $K_{0,pl}$, can be noticeably less than K_{open}.

APPLICATION OF THE MODEL: EFFECT OF LOAD RATIO ON ΔK_{eff}

The inelastic discrete asperities model described in the previous section is now used to analyse the response due to varying load ratios, and also to study the effect of hardness. One effective way to describe the response is to plot the following versus R: (i) the opening stress intensity factor, K_{open} and the corresponding nominal values of the stress intensity factors, $K_{max,nom}$ and $K_{min,nom}$.

(ii) The effective range of stress intensity factor $\Delta K_{\text{eff}} = K_{\text{max,eff}} - K_{\text{min,eff}}$ and the nominal one, ΔK_{nom}, defined according to the usual practice, as: $\Delta K_{\text{nom}} = K_{\text{max,nom}} - K_{\text{min,nom}}$, if $R > 0$ and $\Delta K_{\text{nom}} = K_{\text{max,nom}}$, if $R < 0$. (iii) The asperity height L_i at different R values.

Consider a metal with the mechanical properties typical of aluminium alloy 6061-T6 (baseline material): $E = 69.0$ GPa, $\nu = 0.3$, yield strength $\sigma_y = 300$ MPa, strain-hardening exponent $n = 0.30$ and the constant of Eq. (9), $\sigma_0 = 500$ MPa. The other constant in Eq. (9) that describes the behaviour beyond yield is found by fitting the yield point, i.e. $\varepsilon_0 = (\sigma_y/\sigma_0)^{1/n}$. A single-edge cracked specimen of thickness $t = 10$ mm and width $w = 30$ mm with a crack of length $a = 5$ mm is assumed.

For this case of single-edge through crack of length a in a plate of width w under a remote normal load Q, the stress intensity factor is, e.g. [16]:

$$K_I(Q) = \frac{Q}{wt}\sqrt{\pi a}\left(1.12 - 0.23\frac{a}{w} + 10.6\frac{a^2}{w^2} - 21.7\frac{a^3}{w^3} + 30.4\frac{a^4}{w^4}\right) \tag{19}$$

Consider also a single asperity configuration with an initial interference height $L_0 = 1.5$ μm and initial width $b_0 = 50$ μm. The distance from the crack tip is $C = 90$ μm. Grain size in this aluminium alloy is of the order of 200 μm, therefore the asperity size is a fraction of the grain size. These are typical dimensions of an asperity configuration reported by Carlson *et al.* [17] by fitting the opening stress intensity factor values reported by McEvily and Yang [18]. It should also be noted that typical values of the threshold stress intensity factor range for this type of material are $\Delta K_{\text{thr}} \simeq 4.0\ \text{MPa}\sqrt{\text{m}}$.

To examine the effect of hardness, consider a variation of this baseline material: a 'harder' material with yield strength $\sigma_y = 400\ \text{MN/m}^2$ and the same strain-hardening exponent $n = 0.30$ and $\sigma_0 = 500\ \text{MN/m}^2$.

Load ratios in the range $-2 < R < 0.8$ are examined. In these results, a constant nominal stress intensity factor range $\Delta K_{\text{nom}} = \Delta K_{\text{thr}}$ is maintained by selecting

$$K_{\text{max,nom}} = \frac{(\Delta K_{\text{thr}})}{1-R}; \qquad K_{\text{min,nom}} = \frac{R(\Delta K_{\text{thr}})}{1-R} \qquad \text{if} \quad 0 < R < 1 \quad (K_{\text{min}} > 0)$$

$$K_{\text{max,nom}} = \Delta K_{\text{thr}}; \qquad K_{\text{min,nom}} = R(\Delta K_{\text{thr}}) \qquad \text{if} \quad 0 < R < 0 \quad (K_{\text{min}} < 0)$$

Figure 4(a) shows the nominal stress intensity factors, $K_{\text{max,nom}}$ and $K_{\text{min,nom}}$, as well as the

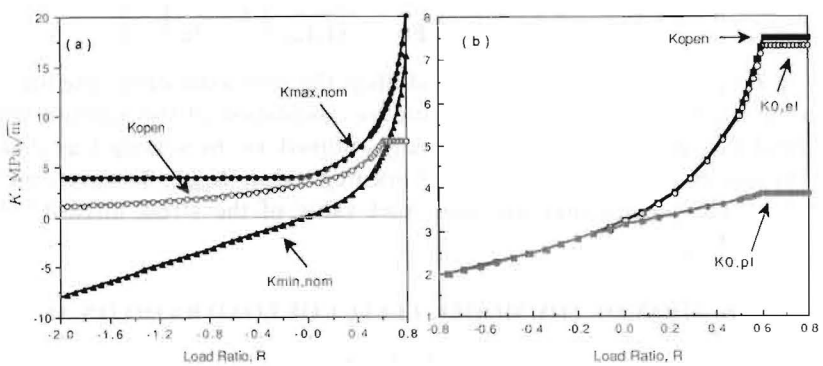

Fig. 4. Load ratio effects. (a) The nominal stress intensity factors, $K_{\text{max,nom}}$ and $K_{\text{min,nom}}$, as well as the opening stress intensity factor, K_{open}, as a function of the load ratio, R. (b) The zero load elastic, $K_{0,\text{el}}$, and plastic, $K_{0,\text{pl}}$, stress intensity factors, in comparison with the opening stress intensity factor, K_{open}, as a function of the load ratio, R.

opening stress intensity factor, K_{open}, as a function of R. Notice that K_{open} is constant for the high positive load ratios, but starts decreasing as the load ratio decreases (once asperity contact is established) and eventually reaches a saturation level for the highly negative load ratios (corresponding to plastic crushing of the asperity). Figure 4(b) shows a comparison of the opening stress intensity factor, K_{open}, with the zero load elastic, $K_{0,el}$ and plastic, $K_{0,pl}$ stress intensity factors. The effect of plasticity is pronounced for the positive load ratios, since for negative Rs, the asperity is already crushed below zero applied nominal load. This plot also shows that K_{open}, in some instance of positive R, may not be a reliable indicator of the effective minimum stress intensity factor.

Figure 5 shows the corresponding $\Delta K_{eff} = K_{max,eff} - K_{min,eff}$ and the nominal $\Delta K_{nom} = K_{max,nom} - K_{min,nom}$ as a function of R. Also, a comparison between the base material and the 'harder' one is shown. By design of the calculations, the nominal ΔK_{nom} was kept constant. Then, it is seen that ΔK_{eff} equals ΔK_{nom} for the high positive load ratios, but decreases as the positive R decreases (corresponding to the increasing influence of closure), reaches a minimum around $R = 0$, and then starts increasing with negative R (corresponding to the plastic crushing of the asperities which reduces closure), reaching again eventually a saturation level below ΔK_{nom}. These curves are qualitatively similar to the ones given by Kemper *et al.* [1], taking into account the fact that in the latter paper the tests were designed so that ΔK_{eff} was constant. In fact, it is easy to conclude from Figs 4 and 5 that if this was the case, ΔK_{nom} would have to increase as the positive load ratio decreases, reaching a maximum around $R = 0$, and then would have to decrease with more negative Rs, eventually reaching a saturation level. It should also be noted that in these calculations, $K_{max,eff} = K_{max}$ and $K_{min,eff} \simeq K_{open}$, i.e. a positive effective minimum stress intensity is developed even with high negative R ratios (and negative nominal K_{min}s).

Figure 6(a,b) shows a comparison between the base material and the 'harder' one. K_{open}, plotted in Fig. 6(a), is larger for the harder material and, accordingly, ΔK_{eff}, already plotted in Fig. 5, is smaller for the harder material (notice that for the high positive load ratios there is no difference). These results reflect the influence of the plastic crushing of the asperity, which is less in the harder material. Hence, closure is a more pronounced phenomenon in the harder material.

Figure 6(b) shows the asperity height L_i/L_0 as a function of R in the two cases (L_0 is the initial asperity height corresponding to the highest positive load ratio). As expected, L_i/L_0 is higher in the harder material, indicating less crushing of the asperity, and therefore more influence of closure on the fatigue behaviour. Kemper *et al.* [1] have performed experiments on the soft recrystallized

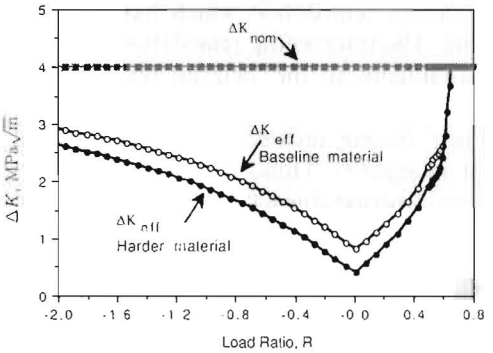

Fig. 5. The nominal stress intensity factor range, ΔK_{nom}, and the effective one, ΔK_{eff}, for the base and harder material, as a function of R.

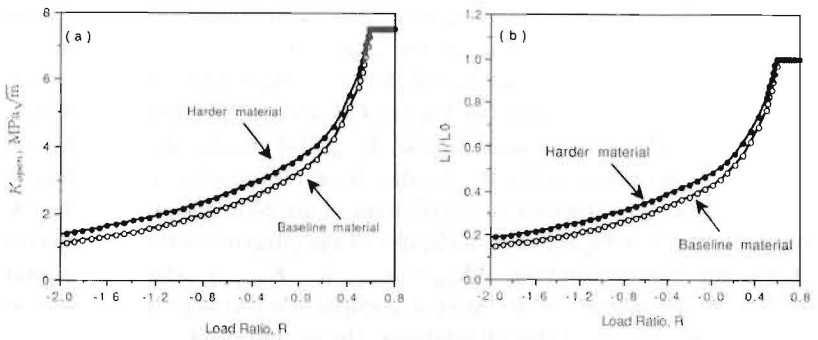

Fig. 6. Hardness effects. (a) The opening stress intensity factor, K_{open}. (b) The asperity height, L_i/L_0, as a function of R, for the base and harder material.

copper and have found the roughness of the fracture surfaces to decrease, indeed, significantly, with decreasing load ratios and at a much faster pace than the harder Al 2024-T3 material.

DISCUSSION

Delayed acceleration and plastic zone effects

The preceding analysis cannot account for transient effects, which have been observed to occur immediately after compressive underloading [6,19]. Thus, although the crushing of asperities may be expected to result in an abrupt growth rate increase by virtue of an increase in the effective range of the stress intensity factor, an initial, transient retardation has been observed. A possible explanation for this transient behaviour may be associated with the sizes of the cyclic plastic zones sizes developed before and immediately after the underloading event. This is illustrated by the cyclic plastic zone size in front of a crack in Fig. 7(a). It is assumed here that the loading prior to and after the application of the underload is under constant ΔK. Immediately after the underloading a new, larger cyclic plastic zone engulfs the zone of Fig. 7(a), as shown in Fig. 7(b). The rate of growth will not resume the rate characteristic of that for Fig. 7(a) until the crack has passed through the larger zone of Fig. 7(b). This is illustrated in Fig. 7(c).

Strain hardening has been cited as a possible contributor to the retardation behaviour which has been observed after tensile overloads [20]. Although this suggestion has not been generally verified, it may be conjectured that the enlarged cyclic plastic zone depicted in Fig. 7(b) may be responsible for the initial, transient retardation which has been observed to occur immediately after compressive underloading. The intervening retardation may, then, be described as a 'delayed acceleration' phase. This is analogous to the 'delayed retardation' designation, which has been observed to occur immediately after a tensile overload.

The phases depicted in Fig. 7 do not include the effects of a reduction of the obstruction to closure due to the crushing of an asperity. Thus, the rate of growth after the above transient effects may be expected to increase for a period during which the steady state obstruction to closure has

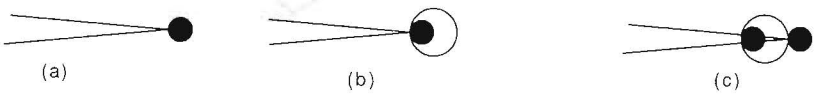

Fig. 7. Cyclic plastic zones: (a) before, (b) immediately after a compressive underload, and (c) after the crack has grown through the underload plastic zone.

been effectively reduced. When the crushed asperities have receded sufficiently from the crack tip, a growth rate characteristic of the constant ΔK may be resumed. It is of interest to observe that the above description suggests that growth rate under variable amplitude loading may therefore consist of a sequence of complex transient behaviours.

One other issue will be discussed now. For the external maximum loads applied, it can be expected that small plastic enclaves would form at the crack tip. Since this can result in a relaxation of the stress state at the crack tip, an estimate of the magnitude of this effect was made. Irwin [21] has proposed the concept of an effective crack length by adding the plastic zone size. This concept was applied to increase the distance from the crack tip to the asperity. Thus, C was increased by the radius of the plastic zone. For plane strain, an estimate of the radius is [22]:

$$R_p = \frac{1}{6\pi}\left(\frac{K_{max}}{\sigma_y}\right)^2 \tag{20}$$

In addition to this tip plasticity effect, one other factor that should be included in analysing compressive underloads, is that the possible intervening crack extension during the compressive excursion phase would tend to increase the growth acceleration of the second positive load ratio phase relative to the first one. Therefore, this crack extension would produce a contribution which opposes the tip plasticity effect.

Residual stress effects

Although the present model has a unique capacity in explaining the observed behaviour when compressive excursions are part of a spectrum loading, it is not the only attempt to examine this subject. A scheme for including the effects of the compressive load excursions has been proposed by Chang *et al.* [23]. They introduced a complex empirical procedure which reduces the plastic zone size used in the Willenborg model [24].

A rational explanation for a Willenborg-type mechanism in the context of compressive excursions may be described as follows. The basic analytical assumption is that the crack surfaces are perfectly flat. A uniformly applied compression can be reasonably expected to produce a uniform, compressive stress state in such a cracked body. In a realistic configuration, however, there can be a void adjacent to the crack tip, which would represent a gap of the type seen in micrographs. Tack and Beevers [8], for example, observed that even under maximum compressive loading, complete closure did not occur. When the presence of such a void is recognized, it follows that the local stress will not be a simple, uniform compression. It could, in fact, result in a very large effective, compressive stress concentration. A very large compressive stress could produce localized compressive yielding. Upon unloading, there would then be a tensile residual stress in front of the crack tip. The tensile residual stress would be superimposed on the stresses produced by the externally applied load.

This mechanism is analogous to that which has been used in experiments designed to initiate cracks. Suresh and Brockenbrough [25], and Tack and Beevers [8] have applied compressive loads to notched specimens to generate residual tensile stress fields which increase the total sensitivity to crack initiation under subsequent cyclic loading. The scales (micro versus macro) for these examples are different, but the mechanisms are similar.

The Willenborg model introduces an effective stress intensity factor which accounts for the presence of a residual stress state. Specifically, for a tensile overload, an effective stress intensity factor K_{eff} is defined as

$$K_{eff} = K - K_R \tag{21a}$$

where K_R is the residual stress intensity factor. For a compressive overload, a change in the sign of the residual stress is formally accounted for by the definition

$$K_{eff} = K + K_R \tag{21b}$$

However, in this approach, no change occurs for the range of the stress intensity factor, ΔK, but the effective stress ratio would be of the form

$$R_{eff} = (K_{min} + K_R)/(K_{max} + K_R) \tag{21c}$$

It should be noted that the K_R of the Willenborg model is not the result of a solution to a mechanics problem, but a rationally evolved, non-unique result, as discussed in Carlson *et al.* [17]. Also, the above definition of R_{eff} does not account for the effects due to closure obstruction. It can be expected that both closure and residual stresses may be present for some loading conditions, particularly in the near-threshold region.

The model discussed in this paper is based on a mechanism that would affect the effective range of the mode I stress intensity factor. The local loads developed between impinging fracture surfaces are not, however, exclusively restricted to mode I effects. Micrographs of fracture surfaces reveal inclined jogs or steps along the crack path. Furthermore, one of the consequences of the misfit developed between the surfaces of growing cracks is the development of contact friction. As has been discussed in Carlson and Kardomateas [4], although the latter may be insignificant for tension–tension tests, they could be important for tests with compressive excursions.

Finally, the proposed model is capable of explaining one additional experimentally observed phenomenon. On specimen loading (unloading the asperities), if the asperities weld to one another, then a tensile force will be developed in the asperities, which would result in a further reduction in the range of the stress intensity factor. This properly describes the differences in growth rates between tests in an inert atmosphere, where welding can occur, and an active atmosphere where welding does not occur [17].

CONCLUSIONS

Experiments have shown that the required stress intensity factor range for growth decreases with increasing positive load ratio, R, values. On the other hand, if the load ratio is negative, it has been observed that the required stress intensity factor range for growth (threshold stress intensity range) decreases as the load ratio becomes more negative, and after a certain point, it remains constant ('saturation' level). It is shown in this paper that these load ratio effects on the fatigue crack growth behaviour can be predicted through a micro-mechanical analysis based on the plastic crushing of a single asperity (or multiple asperities) located on the crack face close to the crack tip. This inelastic discrete asperities model shows, that for a constant applied nominal stress intensity factor range, the effective stress intensity factor range initially decreases as the positive load ratio decreases, reaches a minimum around $R = 0$, and then starts increasing with negative load ratio values, eventually reaching a saturation level below the nominal stress intensity factor range. Another way to describe the effect of asperities is to consider it as a crack-tip shielding mechanism, which is quantified and analysed in this paper. The effect of material hardness and several other related issues, e.g. the residual stresses and plastic zone effects are also discussed.

REFERENCES

1. H. Kemper, B. Weiss and R. Stickler (1989) An alternative presentation of the effects of the stress-ratio on the fatigue threshold. *Engng Fract. Mech.* **32**(4), 591–600.

2. A. McEvily (1977) On crack closure in fatigue crack growth. *Proc. Conf. Fatigue-77*, Metals Science, UK, Vol. 1.
3. J. Radon (1982) Fatigue crack growth in the threshold region. In: *Proc. Int. Conf. Fatigue Threshold*, Stockholm, 1981 (Edited by J. Backlund, A. Blom and C. Beevers), EMAS, UK, p. 114.
4. R. L. Carlson and G. A. Kardomateas (1994) Effects of compressive load excursions on fatigue crack growth. *Int. J. Fatigue* **16,** 141–146.
5. E. Zaiken and R. O. Ritchie (1985) On the role of compressive overloads in influencing crack closure and the threshold condition for fatigue crack growth in 7150 aluminum alloy. *Engng Fract. Mech.* **22,** 35–48.
6. B. Budiansky and J. W. Hutchinson (1978) Analysis of closure in fatigue crack growth. *J. Appl. Mech. (ASME)* **45,** 267–276.
7. J. C. Newman (1981) A crack closure model for predicting fatigue crack growth under aircraft spectrum loading. In: *ASTM STP 748 (American Society for Testing and Materials)*, 53–84.
8. A. J. Tack and C. J. Beevers (1990) The influence of compressive loading on fatigue crack propagation in three aerospace bearing steels. In: *Proceedings, Fourth International Conference on Fatigue and Fatigue Thresholds*, 1179–1184.
9. O. Buck, R. Thompson and D. Rehbein (1988) Using acoustic waves for the characterization of closed fatigue cracks. In: *ASTM STP 982 (American Society for Testing and Materials)*, 536–547.
10. P. J. E. Forsyth (1983) A unified description of micro and macroscopic fatigue crack growth behavior. *Int. J. Fatigue* 3–14.
11. C. J. Beevers, R. L. Carlson, K. Bell and E. A. Starke (1984) A model for fatigue crack closure. *Engng Fract. Mech.* **19,** 93–100.
12. R. L. Carlson and C. J. Beevers (1984) A multiple asperity fatigue crack closure model. *Engng Fract. Mech.* **20,** 687–690.
13. G. A. Kardomateas and R. L. Carlson (1995) An analysis for the effects of compressive load excursions on fatigue crack growth in metallic materials. *J. Appl. Mech. (ASME)* **62,** 240–243.
14. G. A. Kardomateas and R. L. Carlson (1995) An inelastic multiple discrete asperities model for the effects of compressive underloads in fatigue crack growth. *Int. J. Fract.* **70,** 99–115.
15. G. C. Sih, P. C. Paris and F. Erdogan (1962) Crack-tip, stress intensity factors for plane extension and plate bending problems. *J. Appl. Mech. (ASME)* 306–312.
16. K. Hellan (1984) *Introduction to Fracture Mechanics*. McGraw-Hill, New York.
17. R. L. Carlson, G. A. Kardomateas and P. R. Bates (1991) The effects of overloads in fatigue crack growth. *Int. J. Fatigue* **13**(6), 453–460.
18. A. J. McEvily and Z. Yang (1990) Fatigue crack growth retardation mechanisms of single and multiple overloads. In: *Proc. Fourth Int. Conf. on Fatigue and Fatigue Thresholds* (Edited by H. Kitagawa and T. Tanaka), MCEP, Birmingham, UK, 23–26.
19. R. L. Carlson and G. A. Kardomateas (1996) In: *An Introduction to Fatigue in Metals and Composites*. Chapman and Hall, London, 150.
20. R. E. Jones (1973) Fatigue crack growth retardation after single cycle peak overload Ti–6Al–4V titanium alloy. *Engng Fract. Mech.* **5,** 585–604.
21. G. R. Irwin (1960) Plastic zone near a crack and fracture toughness. *Proceedings, Seventh Sagamore Ordnance Materials Research Conference.*
22. F. A. McClintock and G. R. Irwin (1965) Plasticity aspects of fracture mechanics. *ASTM STP 381 (American Society for Testing and Materials)* 84–113.
23. J. B. Chang, M. Szamossi and L.-W. Liu (1981) Random spectrum fatigue crack life predictions with or without considering load interactions. *ASTM STP 748 (American Society for Testing and Materials)* 115–132.
24. J. Willenborg, R. Engle and H. Wood (1971) A crack growth retardation model using an effective stress concept. Report AFFDL-TM-71-1.
25. S. Suresh and J. R. Brockenbrough (1988) Theory and experiments of fracture in cyclic compression: single phase ceramics, transformation ceramics and ceramic composites. *Acta Met.* **36,** 1455–1470.

